ELSEVIER

Chemical Geology 210 (2004) 73–90

CHEMICAL GEOLOGY
INCLUDING
ISOTOPE GEOSCIENCE

www.elsevier.com/locate/chemgeo

Immiscibility between silicate magmas and aqueous fluids: a melt inclusion pursuit into the magmatic-hydrothermal transition in the Omsukchan Granite (NE Russia)

V.S. Kamenetsky[a,b,*], V.B. Naumov[c], P. Davidson[a], E. van Achterbergh[d], C.G. Ryan[d]

[a]*Centre for Ore Deposit Research and School of Earth Sciences, University of Tasmania, Private Bag 79, Hobart, Tasmania, 7001, Australia*
[b]*Max-Planck-Institut für Chemie, Postfach 3060, 55020 Mainz, Germany*
[c]*Vernadsky Institute of Geochemistry, Russian Academy of Science, Kosigin 19, Moscow 117975, Russia*
[d]*CSIRO Exploration and Mining, P.O. Box 136, North Ryde, NSW 2113, Australia*

Abstract

Exsolution (unmixing) of the volatile element-rich phases from cooling and crystallising silicate magmas is critical for element transport from the Earth's interior into the atmosphere, hydrosphere, crustal hydrothermal systems, and the formation of orthomagmatic ore deposits. Unmixing is an inherently fugitive phenomenon and melt inclusions (droplets of melt trapped by minerals) provide robust evidence of this process. In this study, melt inclusions in phenocrystic and miarolitic quartz were studied to better understand immiscibility in the final stages of cooling of, and volatile exsolution from, granitic magmas, using the tin-bearing Omsukchan Granite (NE Russia) as an example.

Primary magmatic inclusions in quartz phenocrysts demonstrate the coexistence of silicate melt and magma-derived Cl-rich fluids (brine and vapour), and emulsions of these, during crystallisation of the granite magma. Microthermometric experiments, in conjunction with PIXE and other analytical techniques, disclose extreme heterogeneity in the composition of the non-silicate phases, even in fluid globules within the same silicate melt inclusion. We suggest that the observed variability is a consequence of strong chemical heterogeneity in the residual silicate-melt/brine/vapour system on a local scale, owing to crystallisation, immiscibility and failure of individual phases to re-equilibrate. The possible evolution of non-silicate volatile magmatic phases into more typical "hydrothermal" chloride solutions was examined using inclusions in quartz from associated miarolitic cavities.

Keywords: Granite; Immiscibility; Melt inclusion; Microthermometry; Nuclear microprobe

1. Introduction

Volatiles dissolved in aluminosilicate magmas (dominantly H_2O, CO_2, S and Cl) play a fundamental role in magmatic evolution across the compositional

* Corresponding author. Centre for Ore Deposit Research and School of Earth Sciences, University of Tasmania, Private Bag 79, Hobart, Tasmania, 7001, Australia. Tel.: +613 62267649; fax: +613 62232547.
E-mail address: Dima.Kamenetsky@utas.edu.au (V.S. Kamenetsky).

0009-2541/$ - see front matter © 2004 Elsevier B.V. All rights reserved.
doi:10.1016/j.chemgeo.2004.06.016

spectrum from komatiite to granite, and in the formation of magma-related hydrothermal systems. Volatiles have a major control on rheological properties of magmas, crystallisation temperature and sequence. When the volatiles exsolve from parental magmas, due to the processes of *unmixing* or *immiscibility*, and form a separate volatile-rich phase (fluid), a major change in the element partitioning occurs. It is believed that volatile phases exsolved during the crystallisation of magmas carry significant amounts of metallic elements (e.g., Candela and Holland, 1984; Shinohara, 1994; Webster, 1997; Kamenetsky et al., 1999; Harris et al., 2003). If dense, these phases may precipitate in situ (e.g., Fe–Cu–Ni–PGE sulphides); if buoyant, they may enter hydrothermal systems and be responsible for formation of certain types of ore deposits (e.g., W–Sn skarns and greisens, pegmatites, and Cu–Mo–Au porphyries).

For many magmas, the evolution of immiscible volatile phases takes place in the poorly characterised interval between the orthomagmatic and the hydrothermal regimes of magmatic cooling and crystallisation. This interval near the magmatic solidus, referred to as *transitional* with respect to processes and compositions (e.g., Burnham and Ohmoto, 1980), has proved extremely difficult to document and understand, largely because of the transient, reactive nature of volatile phases released during magmatic cooling. Also, igneous petrology has long been segregated from studies of hydrothermal systems; although some overlap always existed in the form of experimental and theoretical studies (e.g., Koster van Groos and Wyllie, 1969; Candela, 1989, 1991; Shinohara et al., 1989; Cline and Bodnar, 1991; Webster, 1992, 1997; Shinohara, 1994).

In the case of solidifying felsic magmas, volatile phases are largely exsolved in a temperature window between 850 and 500 °C, that remains virtually "opaque" to geological research. Apart from the problem of how transitional volatile phases eventually acquire the properties of the ore-forming solutions, there are immediate questions about the physical state and chemical compositions of late magmatic fluids. These can be answered by employing melt and fluid inclusion research on samples representative of magmatic-hydrothermal transition (see reviews in Roedder, 1984, 1992; De Vivo and Frezzotti, 1994; Lowenstern, 1995; Frezzotti, 2001; Kamenetsky et al., 2003). Despite the contention that "... interpretation of the inclusion record is commonly ambiguous and difficult, particularly that stage between silicate melt and the hydrous saline melts and aqueous solutions..." (Roedder, 1992), in recent years the melt and fluid inclusion approach has become more attractive and gained strength from the use of modern microbeam techniques (e.g., references in Heinrich et al., 2003; Kamenetsky et al., 2002b, 2003; Kurosawa et al., 2003). In this presentation we studied inclusions in phenocrystic and miarolitic quartz from the Omsukchan granite (NE Russia) to describe an occurrence of immiscibility between the silicate melt and late magmatic volatile phases, characterise their composition from microthermometric experiments and in situ analysis, and attempt to constrain the physical nature and chemical signature of magmatic-derived fluids and their high temperature evolution.

2. Omsukchan granite intrusive

Porphyritic leucogranites of the Cretaceous Omsukchan massif (Chukotka Peninsula, NE Russia) are located within the Okhotsko-Chukotsky volcanic belt and host economic tin deposits. The depth of intrusion defined from the thickness of overlapping volcanisedimentary host rocks was estimated as 0.7–1.5 km (Sokolov, 1980). The intrusion is a flat-topped cupola with shallow-dipping flanks, containing three concentric zones of texturally different granites. Mineralisation is localised in the roof of the cupola, within the zones of metasomatic Na–Fe alteration and quartz-tourmaline veins (Sokolov, 1980). Abundant miarolitic cavities lined with large quartz crystals (to 10 cm) are commonly associated with altered and mineralised granites.

Homogenisation temperatures and salinities of melt and fluid inclusions in quartz and fluorite from granites, miarolitic cavities and metasomatic ore bodies have been previously reported (Naumov and Sokolov, 1981; Kamenetsky et al., 2002b). Temperatures, salinities and compositions were shown to be extremely diverse. To complement the data on inclusions in miarolitic quartz (Kamenetsky et al.,

2002b), the emphasis of this study is on a suite of inclusions in quartz phenocrysts.

3. Inclusions in quartz phenocrysts

3.1. Occurrence of inclusions

Coexisting magmatic inclusions in quartz phenocrysts, unaffected by hydrothermal alteration, are aligned along growth planes and syn-crystallisation fractures. There are three main types of inclusions:

(1) Euhedral crystals of feldspar, mica, sphene, magnetite, apatite, zircon etc. (i.e., minerals cotectic with quartz and accidentally trapped).
(2) Ovoid to spherical inclusions of a magmatic volatile-rich phase (hereafter, *fluid*) that is characterised (at room temperature) by variable proportions of aqueous vapour, liquid and crystals. The endmembers within this type are represented by essentially *vapour* (>90 vol%, Fig. 1a) and dominantly crystalline (>70 vol%, Fig. 1b,c) inclusions. Optical examination revealed at least nine different mineral species (halite and hematite are tentatively identified) present among solids, and often within a single inclusion. In highly crystalline volatile-rich inclusions (hereafter, *brine*) liquid exists interstitially, and a vapour bubble is deformed.
(3) Variable in shape and size, birefringent microcrystalline aggregates of presumably silicate minerals with misshapen vapour phases filling the spaces between solids, and rare opaque phases (Fig. 1d,e), interpreted to be inclusions of crystallised silicate melt. These are commonly surrounded by radiating fractures and halos of tiny vapour-rich aqueous bubbles, suggesting the melt originally had a high volatile content, which was released during post-entrapment crystallisation and decrepitation of these inclusions (Davidson and Kamenetsky, 2001).

As all types of inclusions occur together it is likely that some consist of heterogeneously trapped combinations of cotectic crystals, silicate melt and aqueous fluids. An example of such composite inclusions (crystallised silicate melt and halite-bearing fluid phase) is shown in Fig. 1f.

A number of useful details regarding the phase composition of magmatic inclusions are revealed if the thermometric experiments with inclusions are performed. In this particular case we used approaches described in Kamenetsky et al. (2003).

3.2. Post-heating occurrence of inclusions

Bulk-heating experiments involve heating a quantity of inclusion-bearing quartz phenocrysts in a 1 atm furnace (850–950 °C, 20–50 h) and subsequent air quenching. One objective was to identify those inclusions that were trapped at magmatic temperatures and remained uncompromised (unfractured and unleaked). Bulk heating also revealed inclusions that survived temperature-related volume change of the host quartz (e.g., α-β quartz transition at ~573 °C), and thus were suitable for further microthermometric work. The second aim was to convert crystalline silicate masses within melt inclusions into homogeneous glass. This, in the case of granitic magmas, usually requires long heating times, and eventually makes heterogeneously trapped phases (e.g., fluid, if present) available for observation and analysis. And finally, brine and vapour phases, coexisting with silicate melt, can be coalesced into larger formations (*globules* and *bubbles*, respectively) in order to analyse them using microbeam techniques.

The post-heating examination of the Omsukchan granite quartz phenocrysts reveals the presence of small (<10 μm) bubble-free silicate glass inclusions and larger silicate glass inclusions with one or several low-density vapour bubbles and sometimes unmelted silicate and opaque phases (Fig. 2a). Commonly, the bubbles are located in "swellings" on the otherwise rounded surfaces of such inclusions, and this feature is probably due to differential melting and crystallisation within inclusions during heating and "sheltering" by the bubble of the inclusion wall against crystallisation. The majority of silicate glass inclusions contain spherical globules (Fig. 2c–g) composed of microcrystalline material with variable proportions of spherical to deformed dark phase (vapour). The number (from 1–2 to 10's) and sizes (<1–15 μm) of globules vary significantly. Commonly in larger inclusions these crystal-and vapour-bearing globules

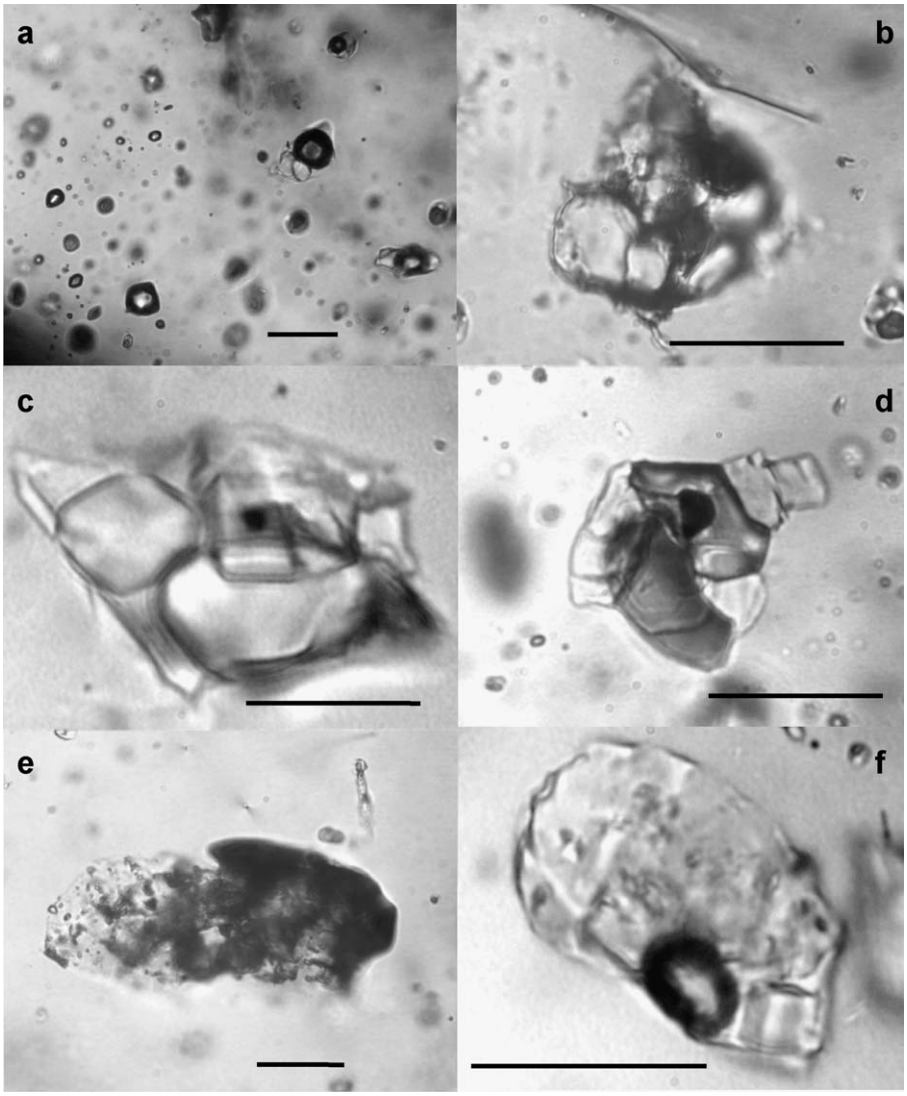

Fig. 1. Magmatic inclusions in quartz phenocrysts: (a) coexisting vapour-rich (dark bubbles) and multiphase brine inclusions; (b, c) multiphase, crystal-rich brine inclusions; (d–f) silicate melt inclusions consisting of birefringent material of different crystallinity, opaques, vapour phases (dark) and sometimes non-silicate minerals. Note cubic crystal, possibly halite, in the lower right corner of the inclusion in (f). Scale bars are 20 μm.

form an emulsion (globules are suspended in the glass "matrix"), and characteristically they are present embedded in the inclusion walls (Figs. 2c,g and 4B) and often without silicate glass, in the host quartz (Figs. 2d,g and 3). Rarely, silicate melt inclusions contain a single, relatively small (~3.5 vol.%) globule,

Fig. 2. Magmatic inclusions in quartz phenocrysts after bulk heating and quenching (see text for details), except in (g) photographed at ~850 °C: (a) silicate glass with shrinkage bubble; (b) composite inclusions consisting of a spherical brine globule and a relatively small amount of silicate glass; (c–g) variable proportions of coexisting brine globules and silicate glass in individual inclusions. Note emulsion texture in (c, f, and g), and the presence of similar brine globules in the host quartz around these inclusions in (d and g). (h, i) microcrystalline structure and deformed vapour phase (dark) of rapidly quenched brine inclusions. Scale bars are 10 μm. Compositions of globules in coexisting inclusions in (e) are in the Table 1 (#3 and #4); PIXE element maps for DK1-7A are shown in Fig. 10B.

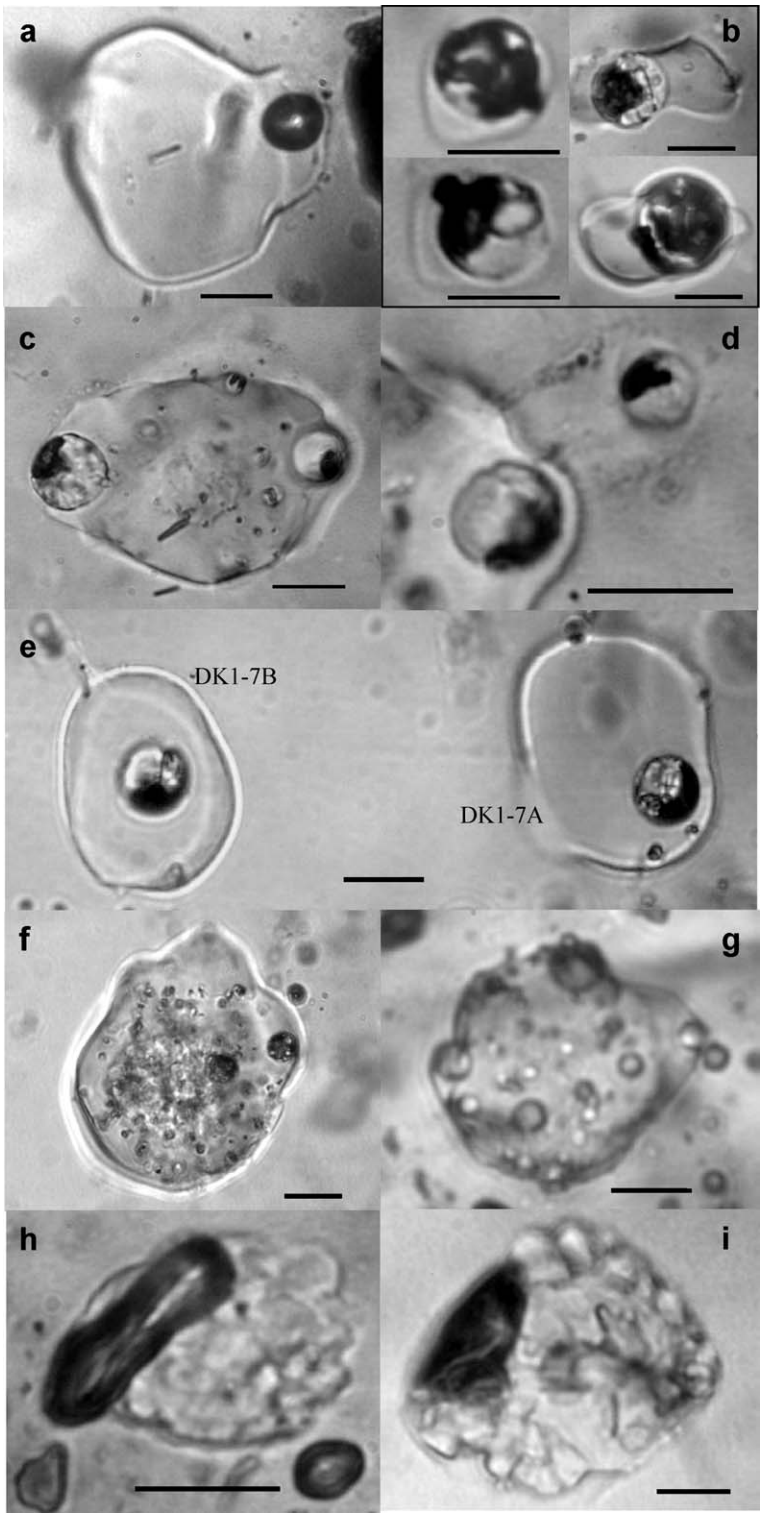
a
b
c
d
e
DK1-7B
DK1-7A
f
g
h
i

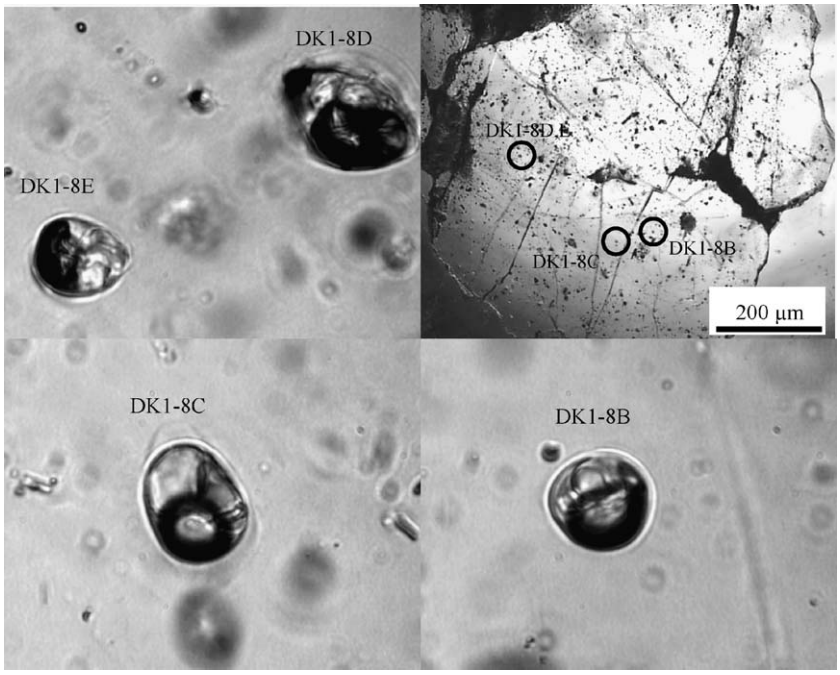

Fig. 3. Spherical and ovoid inclusions of brine in a single quartz phenocryst (positions are circled). Inclusion size is ~10–12 μm. Compositions of inclusions are in the Table 1 (#5–8); PIXE element maps for DK1-8E are shown in Fig. 10C.

as in the two coexisting inclusions shown in Fig. 2e. Other inclusions show a globule (similar to those described above) rimmed by relatively a small volume of the silicate glass (Fig. 2b). And finally, inclusions that contain brine only, are present as negative-crystal shaped inclusions of crystalline material and a deformed bubble (Fig. 2h,i).

3.3. Heating-stage experiments with silicate melt and brine inclusions

Heating-stage experiments were performed to observe, document (e.g., photograph) and register temperature of phase transformations (such as melting, homogenisation, crystallisation, etc.) inside individual inclusions. A Linkam TS1500 heating stage with TMS 94 temperature control unit and an Olympus BX51 microscope with a DP11 digital camera were used. Heating/cooling rates (from 5 to 100 °C/min) were varied when required for more efficient documentation. All grains were first bulk heated in the furnace and quenched (see above). Heating-stage studies targeted spherical globules inside clear silicate glass, and also those trapped in quartz with no silicate glass around them.

Examples of experiments with spherical globules present in the silicate glass are given in Fig. 4. Several subsequent heating runs for each inclusion showed consistent results. Although, the behaviour of all globules studied was very similar, the temperatures of phase transformations in different samples varied. The following general observations were made for spherical globules during heating (Fig. 4):

(1) They remain constant in size, do not change their position with respect to the silicate phase (melt), and do not mix with silicate melt even at temperatures exceeding liquidus (900–1100 °C).
(2) The first visible changes occur at 120–190 °C. These include movement and re-arrangement of solids and the vapour bubble, enhancement of phase boundaries, and the appearance of new phases.
(3) The vapour phase acquires a spherical shape at 250–350 °C, and the boundaries between solid phases become invisible.

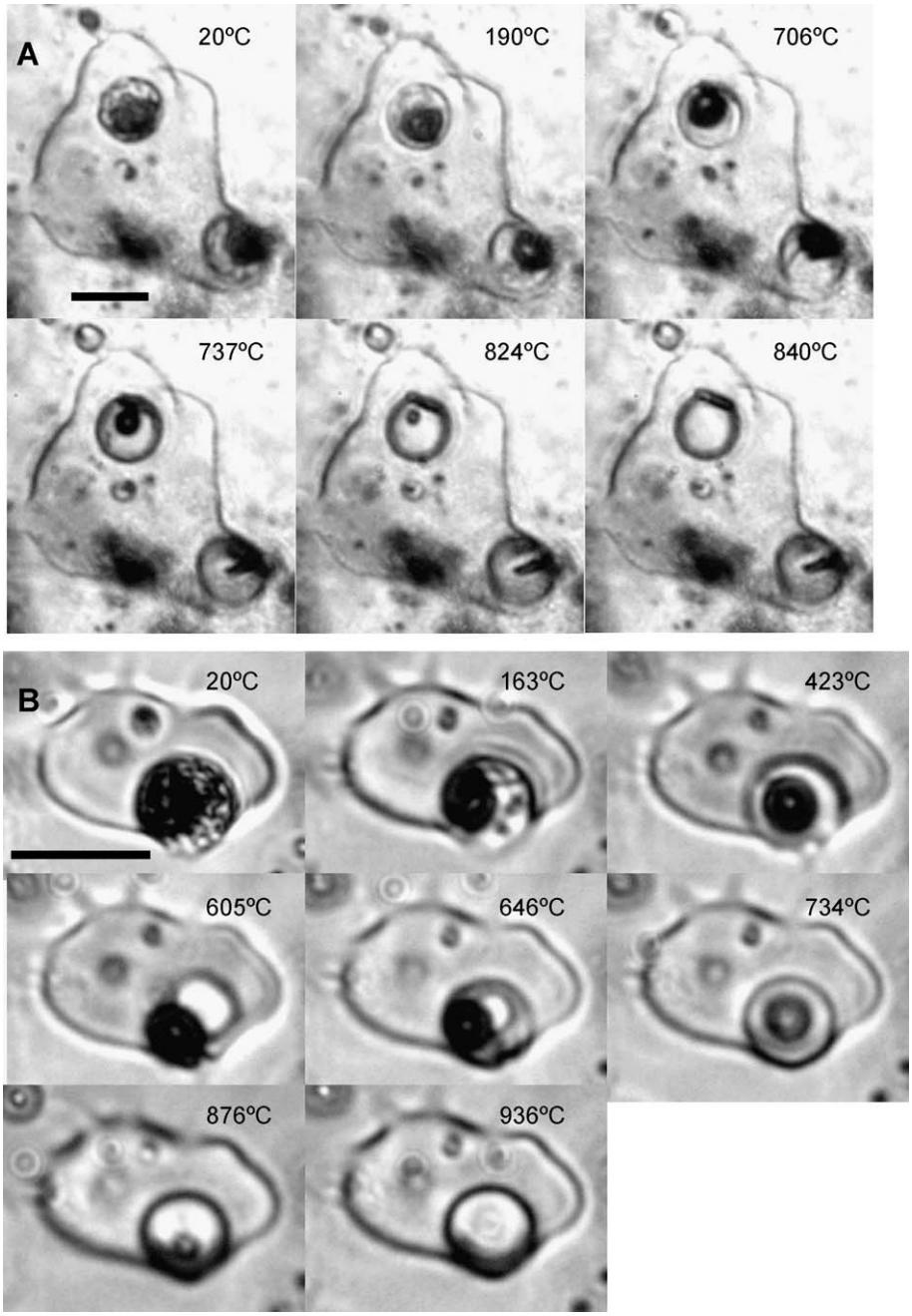

Fig. 4. Phase transformations in spherical brine globules, co-trapped with silicate melt, during heating stage experiments. Scale bars are 15 μm. Compositions of brine globules in the inclusion in (A) are in the Table 1 (#1 and #2); their PIXE element maps are shown in Fig. 10A.

(4) In some inclusions vapour bubbles disappear at 420–510 °C, and then renucleate at ~580 °C. In other globules there is no large change in the bubble size until the quartz transition temperature (~573 °C), in some cases bubbles increase significantly, up to almost the size of the globule.

(5) Melting of solid phase(s) becomes noticeable at >600 °C and is seen as the appearance of liquid (melt) surrounding a cubic crystal.
(6) Heating above 630 °C results in a rapid decrease of the bubble and crystal(s) volumes, with complete melting occurring at 670–735 °C. At these temperatures the liquid in globules has a lower refractive index and lower viscosity than the silicate melt.
(7) Vapour bubbles shrink and move randomly and rapidly, until final disappearance at 790–935 °C.
(8) At the temperature of bubble homogenisation an elongate prismatic brownish crystal, possibly formed as a result of reaction between brine and silicate melt, may remain on the globule-silicate melt interface (Fig. 4A).

It is worth noting that, irrespective of their size, the above phase transformations take place almost simultaneously in all entrapped globules within an individual silicate melt inclusion. This suggests similar compositions and entrapment conditions. The observed differences between globules in different inclusions can be tentatively attributed to the effects of internal pressure.

A record of a typical heating experiment with a spherical brine inclusion in quartz is shown in Fig. 5. In this case, a clear cubic crystal melted at 630 °C, and the melting of a brownish elongate crystal and homogenisation into liquid occurred at 890 °C. The melting and homogenisation temperatures can vary by 100–150 °C for several tens of inclusions studied, even for those within the same quartz phenocryst.

4. Inclusions in miarolitic quartz

Miarolitic cavities within the Omsukchan granite are filled with euhedral quartz crystals that contain numerous populations of inclusions, mainly aligned along syn-crystallisation fractures and more rarely along the growth planes. The majority of inclusions are crystallised Cl-rich fluids (brines), with some vapour-rich inclusions. Silicate melt inclusions have not been recorded. The earlier studies of brine inclusions in the Omsukchan miarolitic quartz (Naumov and Sokolov, 1981; Kamenetsky et al., 2002b) recorded their large size (to 300 μm), high homogenisation temperatures (to 840 °C), and diverse and often metal-enriched chemical compositions. We emphasise the significance of miarolitic brine inclusions for this study is in that they probably represent a magmatic volatile phase that separated from residual melt at the brink of its solidification. Therefore, they

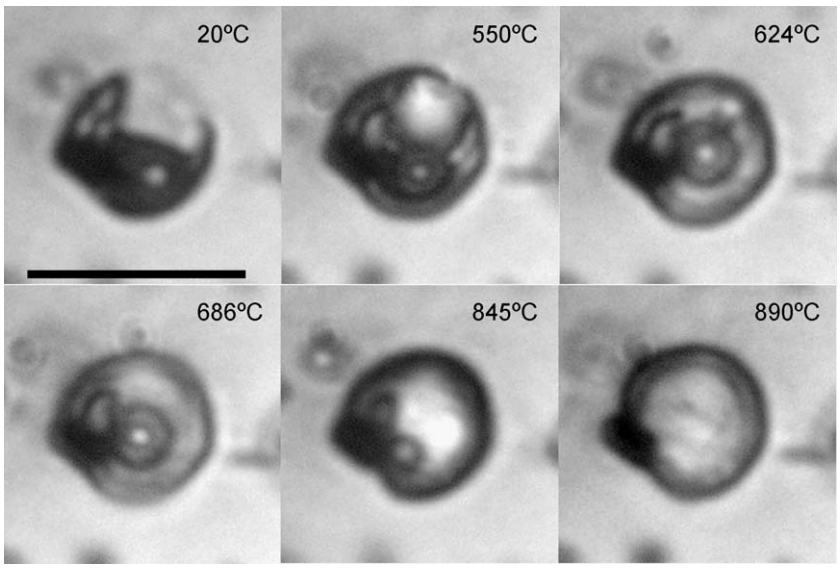

Fig. 5. Phase transformations in the spherical brine globule, entrapped in quartz phenocryst (no silicate glass present), during a heating stage experiment. Scale bar is 15 μm.

can complement the results for the fluids exsolved earlier and trapped as brine globules in phenocrystic quartz. Moreover, the exceptionally large size of miarolitic brine inclusions makes it possible to better document the assemblage of daughter minerals, and phase transformations during heating.

4.1. Inclusion paragenesis

The fact that multiphase brine inclusions belong to the crosscutting trapping planes, and thus to different trapping events (Roedder, 1979), calls for development of criteria for recognition of "assemblages" or "texturally coeval" groups of inclusions. In the following two examples we present descriptions and measurements of phase proportions for inclusions that coexist within a section of the trapping plane (between cross-cutting fractures, Fig. 6A,D), and thus are considered to be trapped simultaneously as a homogeneous solution.

The first example concerns a simple case of the four-phase (liquid+vapour bubble+cubic crystal [halite?]+opaque crystal) inclusions. Despite significantly variable sizes (7–180 μm), 32 measured inclusions in this plane (Fig. 6A–C) have nearly constant volumes of the vapour bubble and cubic mineral relative to the volume of the inclusion (0.127±10% and 0.043±15%, respectively). In the second example (Fig. 6D–F), 34 multiphase (liquid+vapour bubble+3–6 crystals) inclusions of different size (13–120 μm) show similar and constant bubble/inclusion volume ratios (0.127±12%) that in this case seem to be characteristic of homogeneous trapping of fluids. Daughter minerals are typically euhedral, although

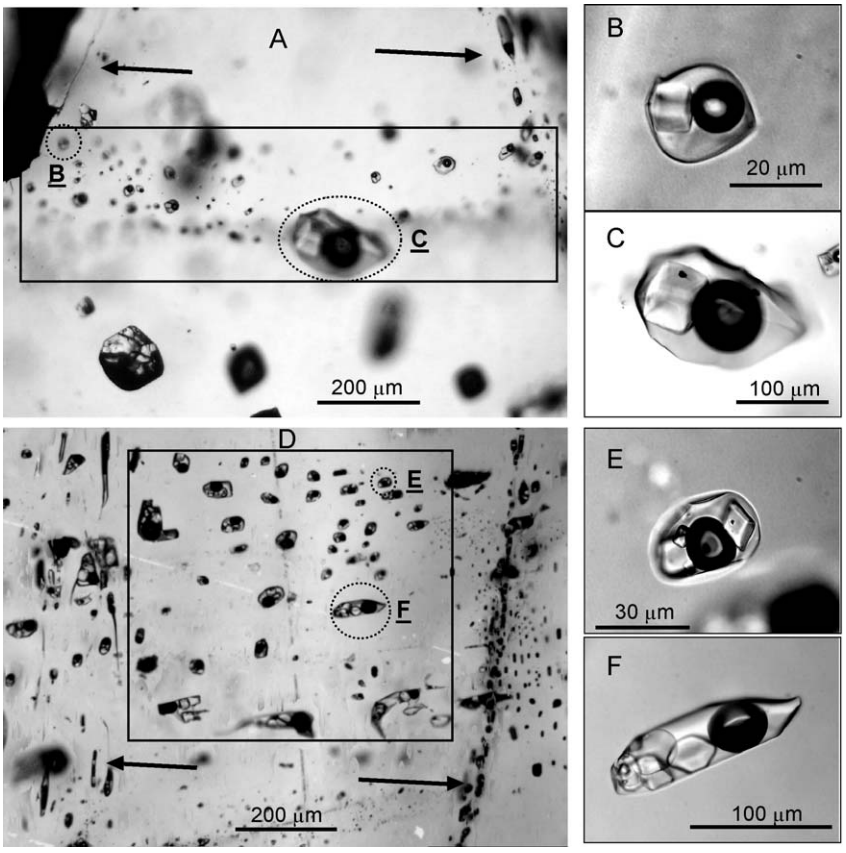

Fig. 6. Multiphase inclusions of aqueous saline fluid within trapping planes in miarolitic quartz. Crosscutting planes are shown by arrows in (A, D). (B, C) and (E, F) representative coexisting inclusions from the trapping planes shown in (A) and (C), respectively (in labelled circles). Similar inclusions were reported by Kamenetsky et al., 2002b.

crystalline aggregates are also present, and show a variety of crystal forms and optical properties, including colour, relief and birefringence (Kamenetsky et al., 2002b). The different appearance of the assemblages of daughter crystals as well as their different compositions (confirmed by laser Raman spectroscopy, Kamenetsky et al., 2002b), are likely to reflect divergent post-entrapment crystallisation paths for individual inclusions. Moreover, even at room temperature the contents of these inclusions are metastable and prone to spontaneous recrystallisation followed by changes in the number, shape and volume ratios of phases (Fig. 7, see also Lowenstern, 1994). This makes it problematic to distinguish between the inclusions belonging to different trapping events.

4.2. Heating-stage experiments with brine inclusions

Due to their small size, the behaviour of spherical brine inclusions in quartz phenocrysts during heating is not fully discernible (Fig. 5). However, as the formation of miarolitic quartz immediately postdated quartz phenocrysts, the microthermometry of larger miarolitic brine inclusions can be cautiously used to characterise earlier granitic brines.

As expected from the variable appearance of inclusions at room temperature (e.g., Fig. 6E,F), the melting behaviour even in those that seemingly belong to the same trapping plane, is also distinct. The summary of general features is as follows (Fig. 8). Most crystals in the multiphase inclusions dissolve below 300–350 °C. The first crystal usually melts at 55–60 °C, the second at 130–150 °C, the third and fourth disappear at 250–300 °C. The large isotropic phase with low relief and cubic shape (presumably halite) melts at 300–625 °C (554 °C in the example in Fig. 8A). Breakdown of some birefringent phases at T~400 °C results in the formation of dispersed dark particles (photo at 390 °C in Fig. 8C) that coalesce into a semi-transparent aggregate of high-relief prismatic crystals (photo at 554 °C in Fig. 8A and photo at 398 °C in Fig. 8C). These newly formed phases start to melt at 620–630 °C, but usually persist to much higher temperatures (~800 °C). Bubbles dissolve at variable temperatures from 380 to 840 °C. In the example shown (Fig. 8A) a bubble first disappeared at 480 °C, then re-appeared at 593 °C (just above the temperature of quartz transition), and disappeared again at 618 °C. Relatively large inclusions (>50 μm) often decrepitate at temperatures below complete homogenisation (photo at 650 °C in Fig. 8B; note that an aggregate of crystals is still present) with the inclusion contents expelled at the grain surface through a fracture. Quenching of the

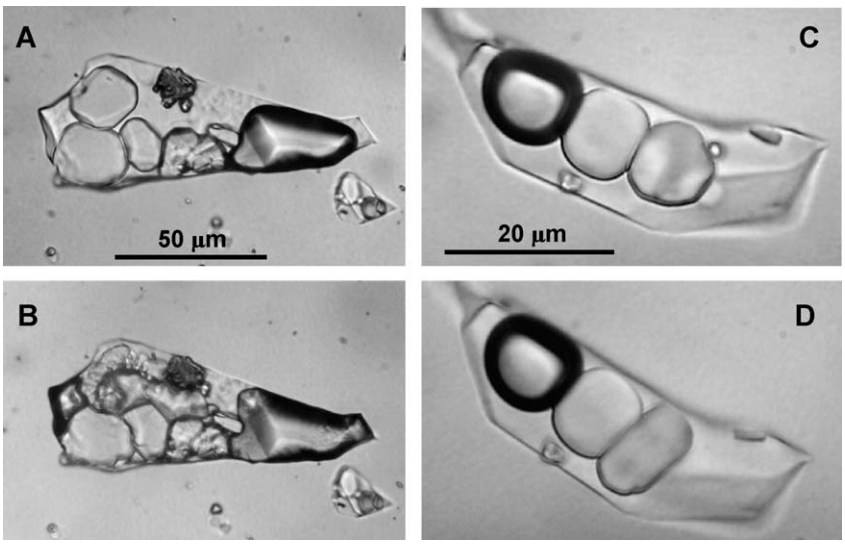

Fig. 7. Metastable nature of multiphase brine inclusions in miarolitic quartz, shown by spontaneous recrystallisation of daughter crystals at room temperature. Photographs of inclusions are taken: (B) 270 days after (A), and (D) 188 days after (C). Similar inclusions were reported by Kamenetsky et al., 2002b.

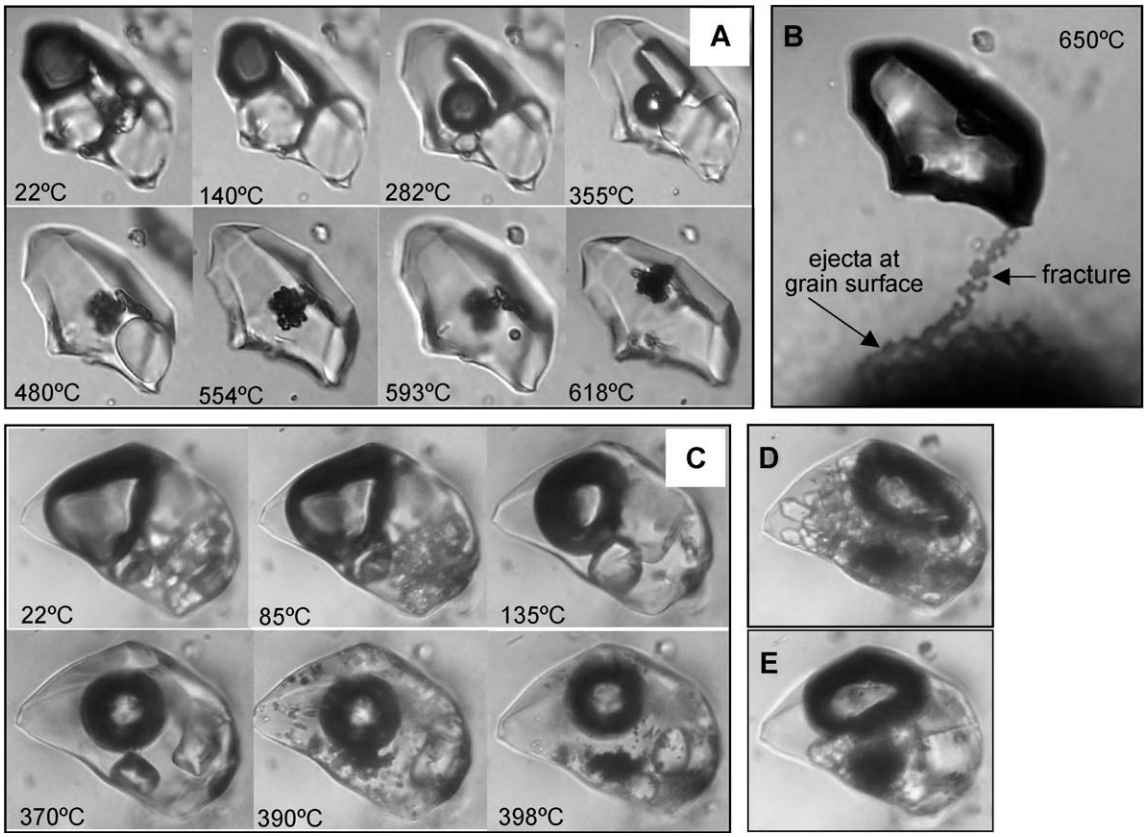

Fig. 8. Phase transformations in multiphase brine globules during heating stage experiments in miarolitic quartz (A and C); (B) decrepitated inclusion shown in (A); (D, E) rapidly (~100 °C/min) and slowly (5 °C/min) cooled inclusion shown in (C). Inclusion sizes are ~60 μm. Similar inclusions were reported by Kamenetsky et al., 2002b.

inclusions results in formation of aggregates of prismatic crystals at <250 °C that almost fill the inclusion (Fig. 8D), whereas slow cooling produces a large cubic crystal (halite?) at <420 °C, followed by spontaneous crystallisation of prismatic birefringent crystals at <200 °C (Fig. 8E).

5. Composition of fluid inclusions

Studied brine inclusions are not quenchable into homogeneous phase (glass) due to the low viscosity of their contents. Thus, at room temperatures the studied inclusions contain aggregates of crystals, a large volume vapour bubble(s) and interstitial aqueous solution (e.g., Figs. 2h,i and 8D,E). There are many difficulties in calculating the bulk inclusion composition based on the compositions of individual phases and their mass proportions, and the most immediate problem is the loss of aqueous and gaseous components when such inclusions are exposed (Kamenetsky et al., 2003). Additionally, the solid content of inclusions is hygroscopic. The analytical methods applied in this case (scanning electron and nuclear microscopy) were partly successful in detecting some elements present and their abundances, although quantitative analysis of fluid inclusions, especially their volatile components, is still under development.

Commonly, inclusions close to the surface of host grains decrepitate during heating and empty their contents on the grain surface (Figs. 8B and 9). We used a scanning electron microscope (Electroscan ESEM2020 equipped with a Link Pentafet SATW energy dispersive X-ray detector, University of Tasmania) to estimate the composition of crystalline and amorphous phases deposited on the surface of

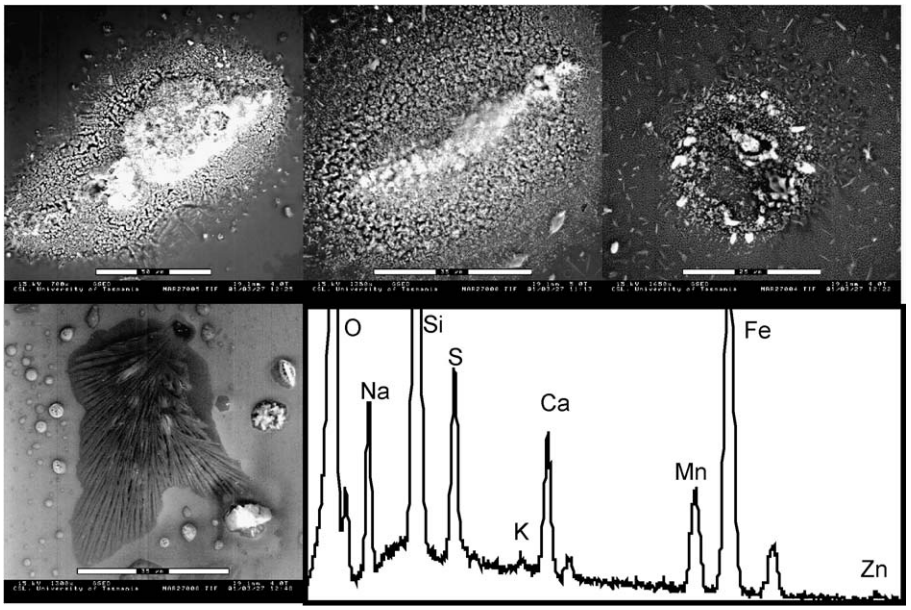

Fig. 9. Scanning electron photomicrographs and representative EDS spectrum of polymineral aggregates crystallised on the surface of miarolitic quartz, from ejected contents of decrepitated during experimental heating fluid inclusions. Elevated abundances of Si in the spectrum are from host quartz.

host quartz as a result of evaporation of the ejecta from decrepitated (bursting) non-silicate inclusions (Fig. 9). Although the ejecta is heterogeneous in phase and chemical composition, it is typically characterised by the dominance of Na, S, Fe, Ca, and Mn. Potassium and Zn are minor components, whereas Cl and Cu are completely missing from the X-ray spectra (Fig. 9). Because some elements are more volatile than others (Cl and Cu in this case) the quantification of the bulk inclusion composition using this method is not possible.

The distribution and abundance of elements heavier than Cl within unopened inclusions were studied by the proton-induced X-ray emission method (PIXE) using the CSIRO-GEMOC Nuclear Microprobe (e.g., Ryan et al., 2001a,b). The PIXE data on the multiphase inclusions in miarolitic quartz, reported earlier (Kamenetsky et al., 2002b), have demonstrated significant concentrations of Cl (up to 50 wt.%), K, Fe and Pb (up to 20 wt.%), Ca (up to 6 wt.%), Mn and Zn (up to 3 wt.%), and Cu, As, Br, Rb, Sr and Sn (up to 1000–3000 ppm). The concentrations of individual elements were 20–90 times higher in the high-salinity (50 wt.% Cl) crystal-rich inclusions compared to the low-salinity (5 wt.% Cl) liquid-rich type. Given the highly variable element ratios in these inclusions a conclusion was made that the granite-derived fluids, if represented by quartz-hosted inclusions, were extremely heterogeneous in composition at the time of quartz growth (Kamenetsky et al., 2002b). These results are complemented in this study by the PIXE element images and concentrations obtained from the spherical brine globules in quartz phenocrysts (Fig. 10 and Table 1). It appears that both types of spherical globules (i.e. trapped with silicate melt and included in quartz) have the same geochemical signature. They are enriched in Cl (and probably Na, not analysed by PIXE), K, Fe, Cu, and to a lesser extent in Ca, Mn, Zn

Fig. 10. Optical images and PIXE element maps of heated inclusions of silicate glass and brine (A, B) and unheated brine inclusion (C) in quartz phenocrysts. Mapping was performed using a 0.3–0.7 nA beam of 3 MeV protons focused into an ~2 μm beam spot with a CSIRO-GEMOC nuclear microprobe (Ryan et al., 2001a,b). Legend shown in lower-right image of (C) indicates relative intensity (and, thus, concentration). Colour scale in each element image is normalised to its own maximum. Outlines on element maps mark boundaries of inclusions and brine globules. Corresponding compositions are given in Table 1: #1 and #2 for shallow and deeper globules, respectively upper and lower globules in (A); #3 for a globule in (B) and #8 for inclusion in (C).

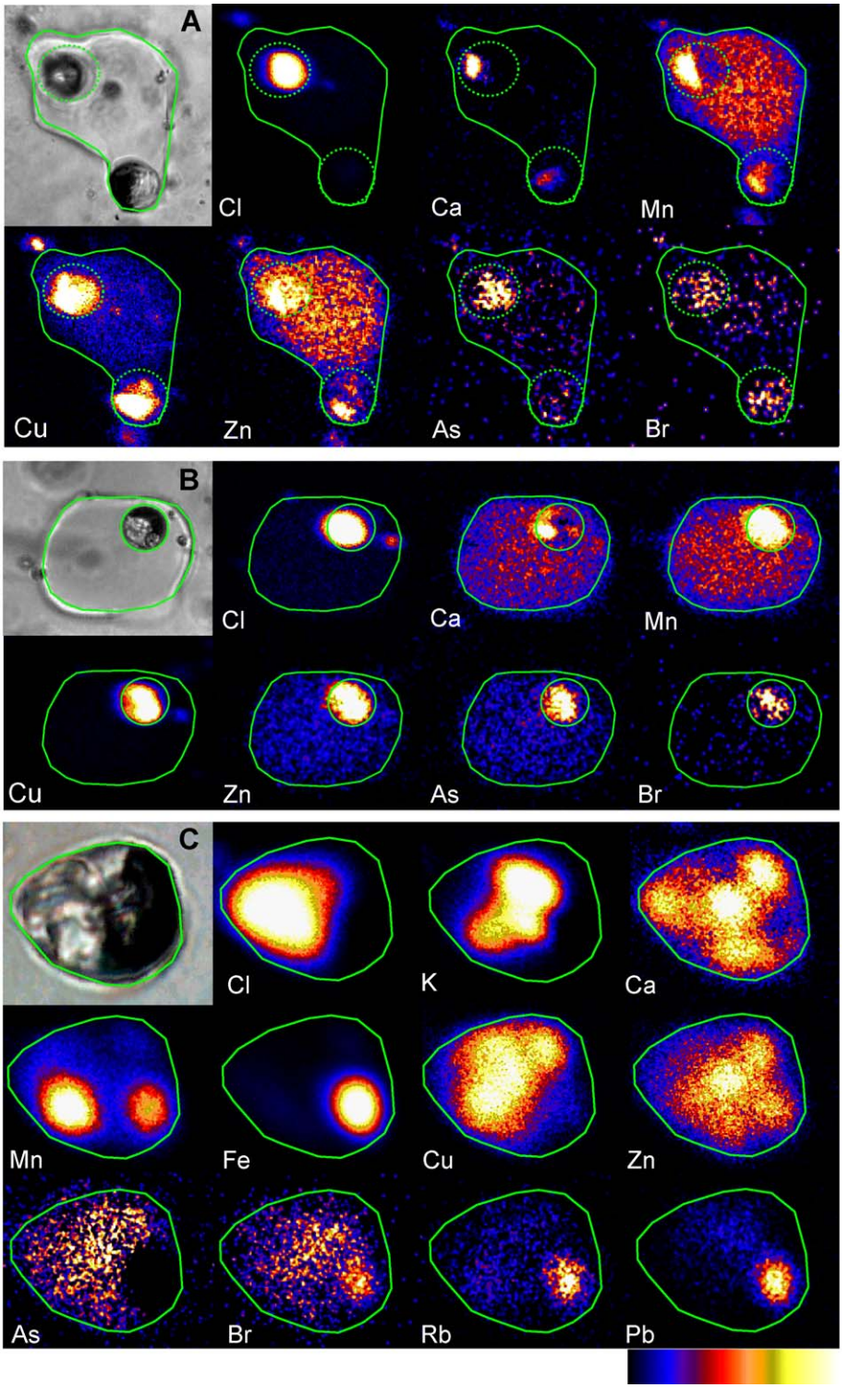
A
Cl
Ca
Mn
Cu
Zn
As
Br
B
Cl
Ca
Mn
Cu
Zn
As
Br
C
Cl
K
Ca
Mn
Fe
Cu
Zn
As
Br
Rb
Pb

Table 1
Compositions and selected element ratios of individual spherical brine globules in quartz phenocrysts, and average composition of multiphase saline fluid inclusions in miarolitic quartz, analysed by nuclear microprobe (PIXE)

	1	2	3	4	5	6	7	8	9	10
Cl (wt.%)	54	15	43	53	7	12	24	12	25	17
K (wt.%)	nq	nq	nq	nq	1.6	2.9	5.0	2.9	5.4	5.0
Ca (wt.%)	0.5	0.8	2.7	0.9	0.9	1.9	1.5	0.9	1.3	1.4
Mn (wt.%)	0.7	0.7	1.2	1.1	0.8	1.4	2.1	1.2	1.0	0.7
Fe (wt.%)	nq	nq	nq	nq	4.0	7.4	19.3	7.9	5.4	4.1
Cu (wt.%)	3.7	6.0	15.4	22.2	2.5	3.6	2.9	1.3	0.024	0.02
Zn (wt.%)	0.5	0.5	0.4	0.5	0.5	0.8	1.3	0.8	0.50	0.36
As (ppm)	1220	470	4300	6550	1160	2030	280	160	226	276
Se (ppm)	1200	300	1430	3830	<50	<100	<100	60	bdl	
Br (ppm)	1080	1450	900	800	590	1040	1300	790	472	329
Rb (ppm)	2050	<670	3480	3620	510	1770	3260	1180	807	713
Sr (ppm)	970	<730	<460	3290	400	590	870	430	253	144
Pb (ppm)	4680	3410	1730	2300	2060	3720	7110	4780	2415	1842
Fe/Cu					1.6	2.1	6.7	6.1	263	158
Mn/Zn	1.4	1.4	3.0	2.2	1.6	1.8	1.6	1.5	2.1	0.6
Zn/Pb	1.1	1.5	2.3	2.2	2.4	2.2	1.8	1.7	2.3	1.2
Cu/Zn	7.4	12	39	44	5.0	4.5	2.2	1.6	0.07	0.10
K/Ca					1.8	1.5	3.3	3.2	5.7	4.4
As/Br	1.1	0.3	4.8	8.2	2.0	2.0	0.2	0.2	0.5	0.4
Pb/Br	4.3	2.4	1.9	2.9	3.5	3.6	5.5	6.1	5.5	3.2
Mn/Br	6.5	4.8	13	14	14	13	16	15	23	9
Cu/As	30	128	36	34	22	18	104	81	2.1	2.1

(1–4)—spherical brine globules co-trapped with silicate melt: (1) and (2)—shallow and deeper globules, respectively, sample DK1-5 (Figs. 4a and 10A); (3) and (4)—globules in coexisting silicate melt inclusions, labelled DK1-7A and DK1-7B, respectively, in Fig. 2e (see Fig. 10B for PIXE maps of DK1-7A). (5–8)—spherical brine globules hosted in a single quartz phenocryst, labelled DK1-8 B, C, D, E in Fig. 3 (see Fig. 10B for PIXE maps of DK1-8E). (9, 10)—average composition and standard deviation for twenty-nine inclusions in miarolitic quartz (Kamenetsky et al., 2002b).
The concentrations were calculated by assuming a bulk density of 1.5 g/cm^3, except (3) and (4) for which a bulk density of 2.0 g/cm^3 was used. PIXE analytical parameters are given in the caption to Fig. 10.
nq—not quantified due to uncertainties caused by the presence of these elements in the host silicate glass; bdl—below detection limit. Analytical uncertainty of the PIXE analyses for the instrument and technique used in this study has been reported to be at 15–30%, with higher uncertainty for elements lighter than potassium (Ryan et al., 1995; see also Kurosawa et al., 2003). Uncertainty depends on internal structure of fluid inclusions (e.g. daughter phases) and their depth from the surface. Note, however, that uncertainties can be reduced if the ratios of elements of similar mass (and with similar X-ray energy), are used in geochemical interpretations.

and Pb. Even elements with concentrations of several hundred ppm (Se, As, and Br) are regarded here as highly enriched relative to their average crustal abundance, and granitic magmas, in particular.

The partitioning of a number of analysed elements between co-trapped silicate melt and brine globules is shown in Fig. 10. The intensity of secondary X-rays for a given element depends on the concentration, density, and depth from the surface. For example, in Fig. 10A the signal from Cl (a relatively light element with low energy X-rays) was strongly attenuated for a deep-seated globule, whereas the intensities of a Cu signal for this, and the shallow globule are comparable. Attenuation of low energy X-rays and uncertainties in the inclusion geometry, depth and density increase the error in the calculated concentrations (Table 1). However, these uncertainties can be reduced if the ratios of elements of similar mass (and with similar X-ray energy), such as Fe and Mn, Cu and Zn, As and Se, etc., are used. The reliability of element ratios, analysed by PIXE, is independently confirmed by the laser ablation ICPMS analyses of brine inclusions (L. Danyushevsky, personal communication).

A number of the element ratios for two globules enclosed within a single silicate melt inclusion (Fig. 10A) are noticeably different (Table 1). Although there exists broad chemical similarity for pairs of spatially associated brine globules in the same quartz phenocryst (Fig. 10C, Table 1, sample DK1-8, pairs of inclusions B–C and D–E as shown in Fig. 3), the average element ratios for each pair of inclusions are significantly different. Furthermore, the comparison between all analysed brine globules in quartz phenocrysts shows considerable variability (>25%) in many element ratios (Table 1).

Tin was detected in brine inclusions in miarolitic quartz in relatively high amounts (up to 1700 ppm). Tin resides in minute crystalline phases that are possibly not cassiterite, as other elements (Cl±As± Mn±Ca) are also present (Fig. 11 and Fig. 3D from Kamenetsky et al., 2002b).

6. Discussion and conclusions

6.1. Evidence for immiscibility

Since the pioneering work on the immiscibility between silicate melts and dense chloride solutions in the Ascension Island granites (Roedder and Coombs,

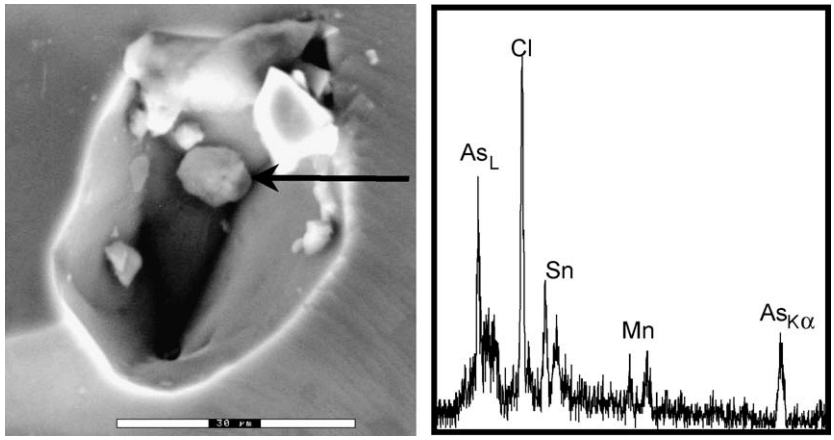

Fig. 11. Scanning electron photomicrograph of a broken surface of miarolitic quartz and an EDS spectrum of the crystal in the cavity of the exposed (presumably) brine inclusion.

1967), only a few studies of intrusive samples have elaborated on the problem of exsolution of brines from, and coexistence with, deep-seated felsic magmas. Specifically, the unambiguous records of the silicate melt and brine co-trapping in a single composite inclusions are provided by the studies of the Mariktikan granite intrusion, Buryatia, Russia (Reyf and Bazheyev, 1977), Monte Genis leucogranite, Sardinia, Italy (Frezzotti, 1992), felsic xenoliths from Ventotene Island, Italy (De Vivo et al., 1995) and quartz veins at Bajo de la Alumbrera porphyry Cu–Au deposit, Argentina (Harris et al., 2003). The reasons for apparent lack of more widespread evidence for the silicate melt-brine immiscibility have been previously discussed (Roedder, 1984, 1992), and we concur that the presence of dispersed, essentially non-silicate phases in the silicate magma is, to a certain extent, disadvantageous for the trapping of silicate melt inclusions. However, we consider the "human factor" more important, for many years these inclusions have not been recognised in quartz from intrusive rocks and "typically hydrothermal" quartz veins. Given the results of this study, we suggest that the application of heating and quenching of several hundred quartz grains should be routinely used to identify the presence of the silicate glass (with or without shrinkage bubbles and heterogeneously trapped volatile-rich phases), otherwise obscured by post-entrapment processes. In the case of quartz phenocrysts from the Omsukchan granite this technique revealed a clear case of immiscibility with at least two liquids simultaneously present during quartz growth, with a meniscus between them. This is best demonstrated by the emulsion textures of many inclusions, in which multiple brine globules (i.e., the dispersed phase) are randomly distributed within silicate glass (Fig. 2c–g) that at the time of trapping was a continuous melt phase from which quartz phenocrysts crystallised. The size of the trapped continuous melt phase is random, largely depending on the size of the growth irregularities on the surface of the host mineral (Roedder, 1984), whereas the size of the trapped dispersed phase is representative of the actual size of the globules (Reyf, 1984). In other words, the size of the brine globules present in the silicate melt inclusions (<1–15 μm; Fig. 2c–g) is characteristic of the size of the natural dispersed phase at the time of immiscibility and before coalescence.

Although heterogeneous trapping of immiscible volatile-rich (fluid) and volatile-poor (silicate melt) phases, as shown by the emulsion textures, is most common in the case of the Omsukchan melt inclusions, some inclusions may still represent homogeneous trapping of either silicate melt or fluid "endmembers" (Figs. 2a,h,i and 3). As the number of pure fluid inclusions exceeds the number of homogeneous silicate glass inclusions by several orders of magnitude, we conclude that the trapping of the discontinuous fluid phase is preferred, possibly because of better wetting properties (Roedder, 1984). Endmember phases present in variable proportions within single two-phase inclusions (Fig. 2b–g) further

imply heterogeneous trapping, especially when the amount of fluid is relatively large (>20%). In cases with only a small proportion of the fluid (Fig. 2e), heterogeneous trapping is less certain because in situ immiscibility is at least possible.

The temperatures of phase transformations and homogenisation within quartz-hosted inclusions recorded in this study ((Figs. 4, 5 and 8); see also Naumov and Sokolov, 1981), although important in generally supporting the presence of essentially non-silicate components in the granitic magma at >650–700 °C, are not applicable to direct quantification of crystallisation temperatures. This is due largely to several unknown parameters controlling internal pressure, and thus experimental temperatures. The most important are the compressibilities of silicate melt and fluid (e.g., Roedder and Bodnar, 1980) and their effect on each other in the case of heterogeneously trapped inclusions, the effects of the $\alpha-\beta$ quartz transition and related microfracturing.

6.2. Compositions of immiscible non-silicate phases

Based on the phase compositions of inclusions in quartz phenocrysts in the Omsukchan granite, the crystallising system consisted of at least silicate melt, Cl-rich fluid (brine) and low-density vapour (Figs. 1–3). We interpret these phases as formed due to immiscibility of the precursor granitic magma that happened before or during quartz crystallisation. Our data are sufficient to resolve whether there was an immiscible fluid of moderate salinity from which vapour and brine formed (Burnham, 1979), or whether vapour and brine were exsolved directly from the magma (e.g., Cline and Bodnar, 1994; Shinohara, 1994; Bodnar, 1995). Based on the fact that two non-silicate, volatile-rich phases (i.e., brine and vapour) have been coexisting with each other and with the silicate melt, we imply that both brine and vapour separated independently, but coevally, from the silicate melt. This provides the most compelling support for the idea that "...granite is only an intermediate stage on a long evolutionary line of melt to 'fluid' compositions. Crystallisation of volatile-bearing granitic magmas can result in a wide range of fluid compositions, at various P, T, and degrees of crystallisation" (Roedder, 1984).

In our study a wide range of "fluid" compositions, as sampled, for example, by brine globules in phenocrystic quartz, is also recorded, despite a limited number of analyses (Table 1). The globules are all metal-rich chloride complexes (Fig. 10, Table 1), although the element abundances and ratios vary significantly, even for co-trapped brine globules (Figs. 4A and 10A). There may be numerous reasons for this, e.g., exsolution of globules (now co-trapped) from different magma batches. But the most immediate is an extreme fractionation of most elements between immiscible silicate melt and non-silicate "fluids" and the disequilibrium character of exsolution. The latter means that if immiscibility is a continuous process, the components of a dispersed phase must have varying composition because of relatively slow diffusion rates. Here we regard disequilibrium as a scale-dependent phenomenon, especially in the residual granitic system, where crystallisation and immiscibility drive chemical fractionation to the extreme. In other words, two adjacent brine globules, formed one after the other, are likely to sample silicate melts of different composition. The difference in the melt compositions, namely the depletion in elements compatible with brine, is caused by their sequestering by the earlier formed brine globule. Moreover, as diffusion rates vary for different elements, even the element ratios in adjacent, consecutively formed globules may be expected to vary (Fig. 10A, Table 1).

It is expected that coalescence of immiscible volatile-rich phases may reduce chemical variability; however, we anticipate that different batches of magmatic fluids have different histories in transit to miarolitic cavities (in effect "fluid chambers") where they accumulate. If this is the case, discrete batches of fluids, following a rock-dominated chemical path (e.g., Heinrich, 1990), are prone to modifications caused by interaction with a granite (solid rocks and residual magma pockets). Moreover, implied unmixing of the fluids due to boiling or effervescence, cooling and related crystallisation, and mixing of fluid batches with each other and possibly external fluids can be responsible for even greater chemical variability, and the change of primary magmatic geochemical signature, as observed in inclusions trapped by miarolitic quartz (Table 1; see also Kamenetsky et al., 2002b). Although some element ratios remain

relatively constant for brine inclusions in earlier phenocrystic quartz, and later miarolitic quartz, the concentration of Cu and proportion of Cu to other metals decrease dramatically in miarolitic brines (from wt.% to hundreds of ppm, Table 1; Kamenetsky et al., 2002b). Such discontinuous evolution and the absence of Cu mineralisation in the Omsukchan granite pose the question whether magmatic fluids in passage to miarolitic cavities experience separation and loss of a vapour-rich phase in which Cu strongly partitions (e.g., Lowenstern et al., 1991; Heinrich et al., 1992, 1999; Lowenstern, 1993; Kamenetsky et al., 2002a; Harris et al., 2003)? Other questions also arise; one is the fate of other economic metals (e.g., Pb and Zn) that are present in significant amounts in brine inclusions but do not form mineralisation. Similarly, despite strong influx of iron during metasomatism of the Omsukchan granite (Sokolov, 1980), Fe sulphides are virtually absent, implying the lack of sulphur in the system.

In conclusion we emphasise that "...formation and evolution of the many different types of immiscible fluids is complex ...but (interpretations) may be of great value in understanding magmatic processes and the resultant ore deposits" (Roedder, 1992), and thus the research into evolution of truly magmatic fluids to hydrothermal solutions is timely, important and will require an international multidisciplinary effort.

Acknowledgements

We particularly recognise the influence of Edwin Roedder, who first understood the potential of melt and fluid inclusion studies in the magmatic-hydrothermal transition, and provided invaluable guidance through his research publications and personal communication. This paper has benefited from discussions with E. Bastrakov, R. Bodnar, T. Crawford, C. Heinrich, J. Lowenstern, T. Sushchevskaya, I. Veksler and J. Webster. We thank Benedetto De Vivo, Jake Lowenstern, Tom Williams and Jim Webster for careful and insightful reviews that significantly improved the manuscript. David Steele helped with the electron microscopy. The research was supported by the Australian Research Fellowship, the Friedrich Wilhelm Bessel Award (Alexander von Humboldt Foundation, Germany) and the Centre for Ore Deposit Research (University of Tasmania) grant to VSK and the Russian Foundation for Basic Research grant 01-05-64109 to VBN. **[SG]**

References

Bodnar, R.J., 1995. Fluid-inclusion evidence for a magmatic source of metals in porphyry copper deposits. In: Thompson, J.F.H. (Ed.), Magmas, Fluids, and Ore Deposits, Miner. Assoc. Canada Short Course Ser., pp. 139–152.

Burnham, C.W., 1979. Magmas and hydrothermal fluids. In: Barnes, H.L. (Ed.), Geochemistry of Hydrothermal Ore Deposits. Wiley, New York, pp. 71–136.

Burnham, C.W., Ohmoto, H., 1980. Late-stage processes of felsic magmatism. Min. Geol. Spec. Issue 8, 1–11.

Candela, P.A., 1989. Calculation of magmatic fluid contributions to porphyry-type ore systems: predicting fluid inclusion chemistries. Geochem. J. 23, 295–305.

Candela, P.A., 1991. Physics of aqueous phase evolution in plutonic environments. Am. Mineral. 76, 1081–1091.

Candela, P.A., Holland, H.D., 1984. The partitioning of copper and molybdenum between silicate melts and aqueous fluids. Geochim. Cosmochim. Acta 48, 373–380.

Cline, J.S., Bodnar, R.J., 1991. Can economic porphyry copper mineralization be generated by a typical calc-alkaline melt? J. Geophys. Res. 96, 8113–8126.

Cline, J.S., Bodnar, R.J., 1994. Direct evolution of brine from a crystallizing silicic melt at the Questa, New Mexico, molybdenum deposit. Econ. Geol. 89, 1780–1802.

Davidson, P., Kamenetsky, V.S., 2001. Immiscibility and continuous melt-fluid evolution within the Rio Blanco porphyry system, Chile: evidence from inclusions in magmatic quartz. Econ. Geol. 96, 1921–1929.

De Vivo, B., Frezzotti, M.L., 1994. Evidence for magmatic immiscibility in Italian subvolcanic systems. In: De Vivo, B., Frezzotti, M.L. (Eds.), Fluid Inclusions in Minerals: Methods and Applications. Short Course of the Working Group IMA. Virginia Tech., Pontignano-Siena, pp. 345–362.

De Vivo, B., Torok, K., Ayuso, R.A., Lima, A., Lirer, L., 1995. Fluid inclusion evidence for magmatic silicate/saline/CO_2 immiscibility and geochemistry of alkaline xenoliths from Ventotene Island, Italy. Geochim. Cosmochim. Acta 59, 2941–2953.

Frezzotti, M.L., 1992. Magmatic immiscibility and fluid phase evolution in the Mount Genis granite (southeastern Sardinia Italy). Geochim. Cosmochim. Acta 56, 21–33.

Frezzotti, M.L., 2001. Silicate-melt inclusions in magmatic rocks: applications to petrology. Lithos 55, 273–299.

Harris, A.C., Kamenetsky, V.S., White, N.C., van Achterbergh, E., Ryan, C.G., 2003. Melt inclusions in veins: linking magmas and porphyry Cu deposits. Science 302, 2109–2111.

Heinrich, C.A., 1990. The chemistry of hydrothermal tin (-tungsten) ore deposition. Econ. Geol. 85, 457–481.

Heinrich, C.A., Ryan, C.G., Mernagh, T.P., Eadington, P.J., 1992. Segregation of ore metals between magmatic brine and vapor: a

fluid inclusion study using PIXE microanalysis. Econ. Geol. 87, 1566–1583.

Heinrich, C.A., Günther, D., Audétat, A., Ulrich, T., Frischknecht, R., 1999. Metal fractionation between magmatic brine and vapor, determined by microanalysis of fluid inclusions. Geology 27, 755–758.

Heinrich, C.A., Pettke, T., Halter, W.E., Aigner-Torres, M., Audétat, A., Günther, D., Hattendorf, B., Bleiner, D., Guillong, M., Horn, I., 2003. Quantitative multi-element analysis of minerals, fluid and melt inclusions by laser-ablation inductively-coupled-plasma mass-spectrometry. Geochim. Cosmochim. Acta 67, 3473–3497.

Kamenetsky, V.S., Wolfe, R.C., Eggins, S.M., Mernagh, T.P., Bastrakov, E., 1999. Volatile exsolution at the Dinkidi Cu–Au porphyry deposit, Philippines: a melt-inclusion record of the initial ore-forming process. Geology 27, 691–694.

Kamenetsky, V.S., Davidson, P., Mernagh, T.P., Crawford, A.J., Gemmell, J.B., Portnyagin, M.V., Shinjo, R., 2002a. Fluid bubbles in melt inclusions and pillow-rim glasses: high-temperature precursors to hydrothermal fluids? Chem. Geol. 183, 349–364.

Kamenetsky, V.S., van Achterbergh, E., Ryan, C.G., Naumov, V.B., Mernagh, T.P., Davidson, P., 2002b. Extreme chemical heterogeneity of granite-derived hydrothermal fluids: an example from inclusions in a single crystal of miarolitic quartz. Geology 30, 459–462.

Kamenetsky, V.S., De Vivo, B., Naumov, V.B., Kamenetsky, M.B., Mernagh, T.P., van Achterbergh, E., Ryan, C.G., Davidson, P., 2003. Magmatic inclusions in the search for natural silicate-salt melt immiscibility: methodology and examples. In: De Vivo, B., Bodnar, R.J. (Eds.), Melt Inclusions in Volcanic Systems: Methods, Applications and Problems, Developments in Volcanology vol. 5. Elsevier, Amsterdam, pp. 65–82.

Koster van Groos, A.F., Wyllie, P.J., 1969. Melting relationships in the system $NaAlSi_3O_8$–NaCl–H_2O at one kilobar pressure, with petrological applications. J. Geol. 77, 581–605.

Kurosawa, M., Shimano, S., Ishii, S., Shima, K., Kato, T., 2003. Quantitative trace element analysis of single fluid inclusions by proton-induced X-ray emission (PIXE): application to fluid inclusions in hydrothermal quartz. Geochim. Cosmochim. Acta 67, 4337–4352.

Lowenstern, J.B., 1993. Evidence for a copper-bearing fluid in magma erupted at the Valley of Ten Thousand Smokes, Alaska. Contrib. Mineral. Petrol. 114, 409–421.

Lowenstern, J.B., 1994. Chlorine, fluid immiscibility, and degassing in peralkaline magmas from Pantelleria, Italy. Am. Mineral. 79, 353–369.

Lowenstern, J.B., 1995. Applications of silicate-melt inclusions to the study of magmatic volatiles. In: Thompson, J.F.H. (Ed.), Magmas, Fluids, and Ore Deposits, Miner. Assoc. Canada Short Course Ser.. , pp. 71–99.

Lowenstern, J.B., Mahood, G.A., Rivers, M.L., Sutton, S.R., 1991. Evidence for extreme partitioning of copper into a magmatic vapor phase. Science 252, 1405–1409.

Naumov, V.B., Sokolov, A.L., 1981. Genetic correlation of granites and the Industrialnoe tin ore deposit according to fluid inclusions data. Geol. Ore Depos. 4, 74–80.

Reyf, F.G., 1984. Microemulsion state of fluid saturated granitic magmas: characteristics and petrological implications. Trans. (Dokl.) USSR Acad. Sci. 276, 1197–1201.

Reyf, F.G., Bazheyev, Y.D., 1977. Magmatic chloride solutions and tungsten mineralizations. Geochem. Int. 14, 45–51.

Roedder, E., 1979. Fluid inclusions as samples of ore fluids. In: Barnes, H.L (Ed.), Geochemistry of Hydrothermal Ore Deposits. Wiley, New York, pp. 684–737.

Roedder, E., 1984. Fluid inclusions. Reviews in Mineralogy vol. 12. Book Crafters, Michigan.

Roedder, E., 1992. Fluid inclusion evidence for immiscibility in magmatic differentiation. Geochim. Cosmochim. Acta 56, 5–20.

Roedder, E., Bodnar, R.J., 1980. Geologic pressure determinations from fluid inclusion studies. Annu. Rev. Earth Planet. Sci. 8, 263–301.

Roedder, E., Coombs, D.S., 1967. Immiscibility in granitic melts, indicated by fluid inclusions in ejected granitic blocks of Ascension Island. J. Petrol. 8, 417–451.

Ryan, C.G., Heinrich, C.A., van Achterbergh, E., Ballhaus, C., Mernagh, T.P., 1995. Microanalysis of ore-forming fluids using the scanning proton microprobe. Nucl. Instrum. Methods Phys. Res., B Beam Interact. Mater. Atoms 104, 182–190.

Ryan, C.G., McInnes, B.M., Williams, P.J., Dong, G., Win, T.T., Yeats, C.J., 2001a. Imaging fluid inclusion content using the new CSIRO-GEMOC Nuclear Microprobe. Nucl. Instrum. Methods Phys. Res., B Beam Interact. Mater. Atoms 181, 570–577.

Ryan, C.G., van Achterbergh, E., Griffin, W.L., Pearson, N.J., O'Reilly, S.Y., Kivi, K., 2001b. Nuclear microprobe analysis of melt inclusions in minerals: windows on metasomatic processes in the Earth's mantle. Nucl. Instrum. Methods Phys. Res., B Beam Interact. Mater. Atoms 181, 578–585.

Shinohara, H., 1994. Exsolution of immiscible vapor and liquid phases from a crystallizing silicate melt: implications for chlorine and metal transport. Geochim. Cosmochim. Acta 58, 5215–5221.

Shinohara, H., Iiyama, J.T., Matsuo, S., 1989. Partition of chlorine compounds between silicate melt and hydrothermal solutions: I. Partition of NaCl–KCl. Geochim. Cosmochim. Acta 53, 2617–2630.

Sokolov, A.L., 1980. Metasomatic zonation of the Industrialnoe-Khatarenskoe ore field (Omsukchan district). Geol. Ore Depos. 2, 27–35.

Webster, J.D., 1992. Water solubility and chlorine partitioning in Cl-rich granitic systems: effects of melt composition at 2 kbar and 800 °C. Geochim. Cosmochim. Acta 56, 679–687.

Webster, J.D., 1997. Exsolution of magmatic volatile phases from Cl-enriched mineralizing granitic magmas and implications for ore metal transport. Geochim. Cosmochim. Acta 61, 1017–1029.